International Journal of Industrial Chemistry (2018) 9:241–253
https://doi.org/10.1007/s40090-018-0153-4

RESEARCH

Application of response surface methodology in the degradation of Reactive Blue 19 using H_2O_2/MgO nanoparticles advanced oxidation process

Shahin Ahmadi[1] · Leili Mohammadi[2] · Chinenye Adaobi Igwegbe[3] · Somayeh Rahdar[1] · Artur Marek Banach[4]

Received: 16 February 2018 / Accepted: 11 September 2018 / Published online: 20 September 2018
© The Author(s) 2018

Abstract

The release of dye containing effluent is a great threat to the world today. The purpose of this study is to optimize the removal of Reactive Blue 19 (RB19) dye from aqueous solutions using advanced oxidation process (AOP). Magnesium oxide nanoparticles (MgO NPs) and hydrogen peroxide (H_2O_2) were used as the catalyst and oxidizer, respectively. Central composite design (CCD) based on response surface methodology (RSM) was applied for optimization of the AOP process. The effects of pH (3–7), molar H_2O_2/MgO NPs ratio (1–3), initial concentration of RB19 (20–80 mg/L), and contact time (30–90 min) were investigated on the oxidation process. The CCD was applied to determine the interactive effects of the process parameters and their optimum conditions. One-way analysis of variance (ANOVA) was applied for statistical data analysis. A quadratic model was generated by the CCD to represent the AOP on RB19 degradation. The experimental values obtained for percentage RB19 decolorization were found to be very close to the predicted response values. Based on the design, optimum conditions of pH 3, contact time of 60 min, RB19 concentration of 80 mg/L and H_2O_2/MgO NPs molar ratio of 3 were obtained which resulted in 93.77% RB19 removal. High value for the coefficient of determination, R^2 (0.912) and adjusted R^2 (0.805) showed that the removal of RB19 dye using AOP can be described by the RSM. The ANOVA results showed that the quadratic model developed from the RSM was statistically significant for RB19 decolorization. From the study, it could be concluded that the RSM can be a useful tool for optimization and moderation of the process parameters to maximize RB19 dye removal from aqueous solutions and the advanced H_2O_2/MgO NPs oxidation process.

Keywords Reactive Blue 19 · Response surface methodology · Advanced oxidation process · MgO nanoparticles · Hydrogen peroxide · Central composite design

Introduction

Nowadays, effluents emanating from industrial actions are one of the biggest problems in the world [1]. Various process industries, such as textile, pulp, and paper, due to the consumption of thousands of colored chemicals in their production activities are significant sources of dye pollutants in the environment [2]. The global consumption of organic dyes is estimated to be over 700,000 tons per year, and textile consumption is 75% [3]. Water consumption for production in the textile industry is estimated between 100 and 200 L/kg, which result in very high volumes of wastewater containing acids, alkali, toxic compounds as well as colored materials [3, 4]. Colorants are typical of artificial origin with a complex molecular structure derived from coal tar, which contains hydrocarbons such as benzene, naphthalene, anthracene, toluene, and glycine [5].

✉ Shahin Ahmadi
sh.ahmadi398@gmail.com

✉ Chinenye Adaobi Igwegbe
ca.igwegbe@unizik.edu.ng

✉ Artur Marek Banach
abanach@kul.pl

[1] Department of Environmental Health, Zabol University of Medical Sciences, Zabol, Iran

[2] Promotion Research Center, Zahedan University of Medical Sciences, Zahedan, Iran

[3] Department of Chemical Engineering, Nnamdi Azikiwe University, Awka, Nigeria

[4] Department of Biochemistry and Environmental Chemistry, Institute of Biotechnology, The John Paul II Catholic University of Lublin, Konstantynów 1I Str, 20-708 Lublin, Poland

Reactive dyes are soluble anionic dyes. After the azo dyes group, they are the most widely used colorants in the textile industry [6]. These dyes have been used to replace direct, azo, and Watts dyes because of their desirable properties such as transparency and low energy consumption [7].

The reactive dye, with its characteristic chemical structure, is normally resistant to chemical attack and has a small stabilization effect due to the competition between the formation of its reactive state (vinyl sulfone) and hydrolysis reactions [8]. They can pose a negative impact on the environment due to the reduction in light penetration and impairment of photosynthesis process [9, 10]. Reactive Blue 19 (RB19) also known as Remazol Brilliant blue is an anthraquinone dye used by the textile industries [11]. Therefore, the removal of the dye from wastewaters is of great necessity. Removal of color is possible through various physical, chemical, biological methods or a combination of them [12].

Several treatment methods have been proposed for the removal of RB19 from contaminated waters, which include photodecomposition [13], electro-coagulation [3] adsorption [14], dissolved air flotation [15], biodegradation [16], and other processes. The afore-mentioned methods cause problems such as their control, injection of chemicals and production of high volumes of sludge with attendant problems of filtration and sludge disposal [17]. Advanced oxidation process (AOP) is highly effective in the removal of organic compounds because of its high efficiency and high oxidation potential [18, 19]. The AOP generally refers to a process in which a catalyst such as magnesium oxide, and a strong oxidizing agent such as hydrogen peroxide and ozone are used in the presence or absence of an ultraviolet radiation source [18, 20]. This process results in the production of free and active radicals (OH). The hydroxyl ion is very significant due to its high oxidation power and the reduction in environmental pollution caused by organic matter [21, 22]. This method is applicable to the degradation of resistant compounds in comparison to other methods and, in view of its high oxidizing power; it converts them into mineral forms under special conditions [23]. In addition, recent advances on the removal of dyes using Fe-based metallic glasses/AOPs are also attractive [24–26]. Among different oxidation processes, hydrogen peroxide (H_2O_2)/nanoparticles oxidation process is a novel technology in which toxic materials are degraded to harmless compounds [17]. H_2O_2 is a common oxidizing agent that generates $^{\cdot}OH$ radicals and oxidizes organic and inorganic materials with high oxidizing capacity [27]. Magnesium oxide nanoparticles (MgO NPs) were used as a catalyst in the purification of dangerous, antibacterial and resistive materials [28].

The significant characteristics of MgO NPs include availability, low cost, non-volatility, non-toxicity, stability, high adsorption capacity and high reactivity [29]. For this reason, it is an appropriate option used for remediation processes.

The purpose of this study is to optimize the removal of RB19 dye from aqueous solutions via AOP using MgO NPs. The central composite design (CCD) based on response surface method (RSM) was used to design the experiments for RB19 decolorization. It is an important branch of empirical design and basic tool in developing new processes, optimizing their performance and improving the design and formulation of new products [30, 31]. RSM was also applied to investigate the individual effects of the process variables and their relationship or interactions to maximize the efficiency of RB19 decolorization as well as determine the optimal conditions. The test system used is a discontinuous type and the variables studied include the solution pH, H_2O_2/MgO NPs molar ratio, concentration of RB19, and time of reaction.

Materials and methods

Materials

NaOH (98%), HCl (37%) and H_2O_2 (30%) used in the study were of analytical grade (supplied by Sigma-Aldrich Co, Germany). RB19 is an anionic dye with a molecular weight of 626.54 g/mol and maximum absorption (λ_{max}) of 594 nm. The RB19 ($C_{22}H_{16}N_2Na_2O_{11}S_3$) used in this work was of analytical grade (supplied by Sigma-Aldrich—US). The magnesium oxide nanoparticles (MgO NPs) of 98% percentage purity and 50 nm size were purchased from Sigma-Aldrich (US).

Characterization of MgO NPs

Fourier-transform infrared spectroscopy (FTIR) was done on a JASCO 640 plus machine (4000–400 cm^{-1}) at room temperature to examine the functional groups present in the MgO NPs, which took part in the AOP for RB19 decolorization. Value-stream mapping (VSM) was also performed on the MgO NPs. Vibrating magnetometry (VSM) was analyzed using a Kavir Precise Magnetic instrument (MDKFT, Iran). X-ray diffraction (XRD) was determined using an X-ray diffract meter with XRD SMART Lab to evaluate the crystalline properties of MgO NPs.

Batch experiments

Magnesium oxide nanoparticles (MgO NPs) were used as the catalyst while hydrogen peroxide (H_2O_2) was used as the oxidizer for the process. The effect of the oxidation process parameters, pH (3–7), molar ratio of H_2O_2/MgO NPs (1–3), initial concentration of RB19 (20–80 mg/L), and contact time (30–90 min) on the process were investigated. All stock solutions of RB19 were prepared with double-distilled

water. Batch experiments were conducted in 250 mL Erlenmeyer flasks to study the removal of RB19 by AOP. First, the RB19 stock solution was prepared and then the samples with different concentrations (20, 40, 60 and 80 mg/L) were prepared from the stock. The pH of the solution was adjusted by adding 0.1 N HCl or NaOH solutions. The pH was measured using an MIT65 pH meter. A specific amount of catalyst (MgO NPs) and oxidizer (H_2O_2) were added to the color solution with a specific initial RB19 concentration and placed on the shaker and blended. All solutions underwent constant mixing at the 180 rpm for 2 h. After the desired time of mixing, the mixture was filtered using the Whatman filter paper (size: 40 µm). Then, the filtrate was analyzed for the residual RB19 concentration. The initial and final RB19 concentrations remaining in solutions were analyzed by a UV–visible recording spectrophotometer (Shimadzu Model: CE-1021-UK) at a wavelength of maximum absorbance, $\lambda_{max} = 595$ nm. Percentage of decolorization was calculated as follows [32, 33]:

$$\text{Decolorization}\,(\%) = \frac{(C_0 - C_f)}{C_0} \times 100, \tag{1}$$

where C_0 and C_f are the initial and final RB19 dye concentration, respectively.

Design of experiments and statistical analysis

The response surface methodology (RSM) is an effective method for the optimization of processes. The RSM method can be employed on the basis of different designs including CCD, Box–Behnken design (BBD), one-factor design, d-optimal design, etc. [34]. In the study, the CCD was applied to evaluate the impact of the independent variables [pH, H_2O_2/MgO NPs ratio, time and initial concentration of RB19 on the dependent variable (RB19 decolorization, %)]. The CCD was applied using Design Expert software (Stat-Ease, 7.1 trial version). Four factors at three levels of full factorial CCD based on RSM was used which gave a total of 30 experiments (including 8 axial points, 16 factorial points and 6 replicates at the center points) to optimize the chosen variables. The experimental range of the contributory factors and selected levels of the independent variables used in the study are presented in Table 1.

The fitting on the efficiency of eliminating color was implemented using the coefficient of determination (R^2) and the adjusted R^2. Furthermore, analysis of variance (ANOVA) was applied as a statistical method to analyze the responses and to understand better the effects of variables. The reason for using this statistical model is due to the high expense of nanoparticles, sample shrinking size, and presentation of linear equation. The experimental settings, which were designed using CCD for the assessment of the effect of several factors and optimization of process parameters, are presented in Table 2. The response, *Y,* can be represented by a mathematical equation that correlates the response surface. The response, *Y,* can be expressed as a polynomial model based on the following quadratic equation [35, 36]:

Table 1 Experimental range and levels of independent variables tested

Factor	Independent variables	Unit	Range and level of actual and coded values		
			−1	0	+1
A	Initial pH	–	3	5	7
B	Initial RB19 concentration	mg/L	20	50	80
C	Time	min	30	60	90
D	H_2O_2/MgO NPs ratio	mg/L	1	2	3

$$\begin{aligned} Y = {} & b_0 + b_1A + b_2B + b_3C + b_4D + b_{11}A^2 \\ & + b_{22}B^2 + b_{33}C^2 + b_{44}D^2 + b_{12}AB \\ & + b_{13}AC + b_{14}AD + b_{23}BC + b_{24}BD + b_{34}CD \end{aligned} \tag{2}$$

where Y represents the predicted response (RB19 percentage decolorization); A, B, C and D are the coded values of the independent process factors: initial pH of solution, initial RB19 concentration, reaction time and H_2O_2/MgO NPs ratio, respectively. b_0, b_1, b_2, b_3, b_4, b_{11}, b_{12}, b_{13}, b_{14}, b_{22}, b_{23}, b_{24}, b_{33}, b_{34}, and b_{44} are the constant regression coefficients.

ANOVA was used to evaluate the significance of the quadratic regression model. Also, the model terms were assessed using the p value with 95% confidence level. The coefficient parameters were assessed by response surface regression analysis using the software Design Expert (version 7). It was also applied to obtain the residuals, 3-D surface and 2-D contour plots of the response models.

Results and discussion

Magnetization characterization of catalyst

Value-stream mapping is a lean management technique for examining the present state and designing an impending state for the series of events that take a product or service from its beginning through to the customer. Magnetization measurements of the catalyst, magnesium oxide nanoparticles (MgO NPs) were done using the VSM technique at fields of − 8000 to 8000 emu/g (before and after calcination, respectively) operated at room temperature (see Fig. 1). It was observed that MgO NPs produced a higher value of

Table 2 Experimental design matrix with the experimental and predicted values for RB19 discoloration efficiency (%) using AOP

Run	Initial pH (*A*)	Initial RB19 concentration (*B*)	Time (*C*)	H_2O_2/MgO NPs ratio (*D*)	Experimental % decolorization	Predicted % decolorization
1	3	80	60	2	85.36	78.563
2	3	80	30	3	71.13	81.64
3	5	60	60	1	91.7	95.201
4	3	20	90	3	72.19	80.342
5	3	50	30	1	27.8	33.059
6	3	20	60	2	81.61	76.246
7	3	50	30	3	94.9	72.244
8	3	20	30	1	8.96	11.622
9	3	60	90	2	53.28	64.687
10	3	80	90	1	64.04	55.271
11	5	60	60	2	92.67	88.121
12	7	60	60	2	93.42	93.42
13	3	80	90	3	85.2	81.533
14	3	20	90	3	72.19	67.706
15	5	60	60	3	92.6	93.767
16	5	60	60	2	92.67	90.329
17	3	20	30	3	17.26	28.36
18	3	20	90	1	65.02	61.403
19	3	80	30	3	71.13	73.86
20	5	60	60	2	92.67	92.028
21	3	50	60	2	87.78	91.072
22	3	80	90	1	64.04	71.618
23	3	60	30	1	44.31	44.877
24	5	60	60	2	92.6	93.668
25	3	20	90	1	65.02	61.273
26	5	60	60	2	92.67	94.466
27	3	60	60	2	92.82	101.69
28	3	80	90	3	85.2	82.347
29	3	60	30	2	45.51	38.771
30	3	80	30	1	52.41	48.976

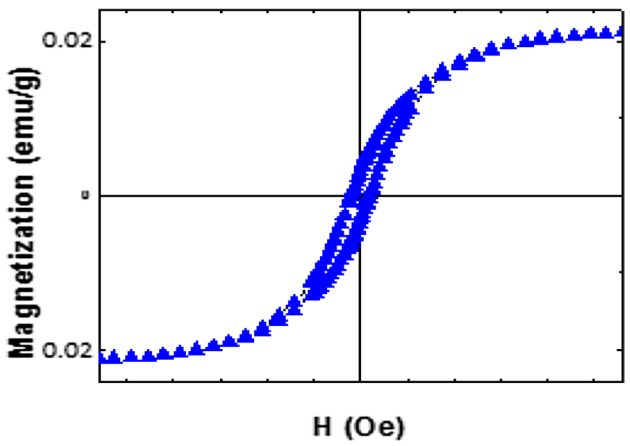

Fig. 1 VSM hysteresis loop of magnetic MgO NPs

saturation magnetization (0.02 emu/g) with the smallest particle size.

Fourier-transform infrared spectroscopy (FTIR) spectroscopy

Figure 2 shows the FTIR spectrum (%transmittance versus wave number) for MgO NPs. The functional groups present in MgO NPs (which took part in RB19 decolorization) were identified. The peak of 1615.92 cm^{-1} [C–C stretching (in-ring) is assigned to aromatics, 1384.58 cm^{-1} (N=O bending] shows the presence of nitro compounds, 1087.17 cm^{-1} (C–N stretching) is assigned to aliphatic amines, 3700.56 cm^{-1} (C–N stretch) indicates aliphatic amines. Peaks 3419.46 cm^{-1} (O–H stretch, H–bonded) assigned to alcohols and phenols are very strong and broadband which also took part actively in the decolorization of RB19.

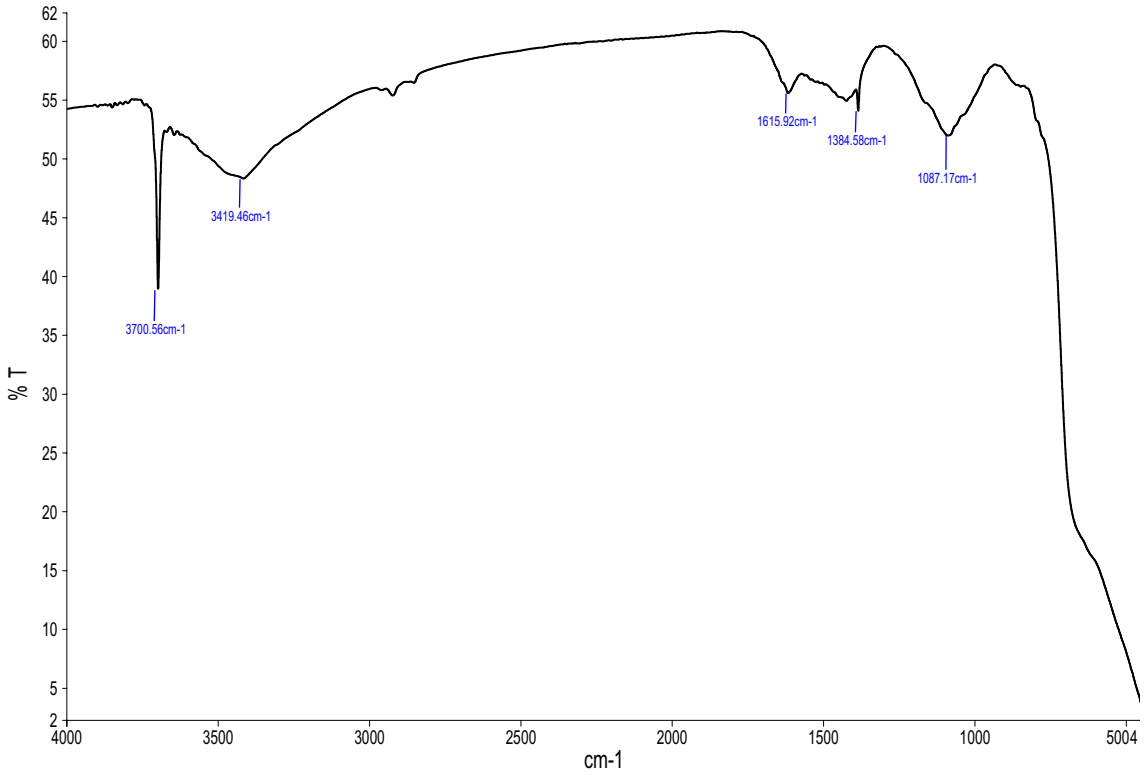

Fig. 2 FTIR spectrum of the MgO NPs

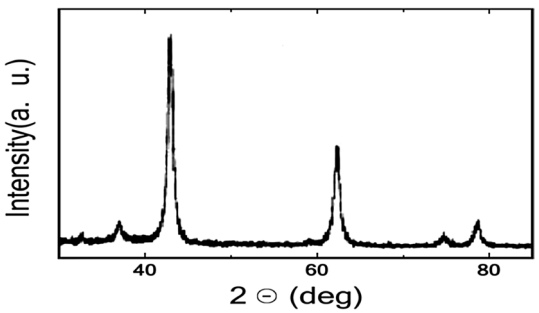

Fig. 3 XRD patterns of MgO NPs

X-ray diffraction study

X-ray diffraction was done to determine the diffractive pattern of MgO NPs. Figure 3 shows the XRD pattern of MgO NPs. Broad peaks were observed on the XRD image which indicates the presence of crystalline constituents in the NPs. The XRD image showed that the maximum peak is about 43° with extremely high intensity.

Model fitting and statistical analysis of RB19 decolorization using RSM

The first step in this study was to identify the variables that influenced the decolorization process and their range. Thus, initially, the capacity of H_2O_2/MgO NPs ratio was tested in the decolorization of RB19 at pH 3, 5 and 7 while keeping other process variables constant. It was found that the H_2O_2/MgO NPs ratio was only able to decolorize the dye RB19 at pH 3 and the decolorization obtained was 95% at 60 min. Then, the experimental runs were performed according to the operating parametric values given in Table 2. The experimental results were analyzed using RSM to obtain an empirical model for the best response. The actual and the predicted dye decolorization percentages are shown in Table 2. The actual values were found to be close to the predicted values evaluated from the model for a specific run.

In order to develop a statistically model, the significance of the coefficients of regression was determined in relation to the p values. From Table 3 (the ANOVA results), the quadratic model developed from the RSM was statistically significant for RB19% decolorization (Y). A p value less than 0.05 indicate that the effect of a term is significant. The model F value of 9.37 and Prob > F value less than 0.0500 implies that the model is significant for RB19 decolorization. Low value of Prob > F (less than 0.05) indicates

Table 3 ANOVA, lack-of-fit (LOF) test, and regression coefficients and the significance of the response surface quadratic model of AOP decolorization of the dye solution

Source	Coefficients	Sum of squares	Degree of freedom (*df*)	Mean square	F value	*p* value Prob > *F*
Model	79.51	14400.77	12	1200.06	9.37	< 0.0001
A-pH	− 13.34	271.14	1	271.14	2.12	0.1639
B-concentration	6.40	521.06	1	521.06	4.07	0.0598
C-time	− 41.28	1187.10	1	1187.10	9.27	0.0073
D-H_2O_2/MgO NPs	1.20	5.16	1	5.16	0.040	0.8434
AB	–	0.000	0	–	–	–
AC	–	0.000	0	–	–	–
AD	− 11.53	448.57	1	448.57	3.50	0.0786
BC	− 13.07	965.92	1	965.92	7.54	0.0138
BD	1.81	79.64	1	79.64	0.62	0.4413
CD	− 3.90	194.21	1	194.21	1.52	0.2350
A^2	5.35	54.16	1	54.16	0.42	0.5243
B^2	− 16.09	654.52	1	654.52	5.11	0.0372
C^2	− 91.49	2794.96	1	2794.96	21.82	0.0002
D^2	8.07	283.15	1	283.15	2.21	0.1554
Residual	–	2177.95	17	128.11	–	–
Lack of fit	–	2177.95	8	272.24	6.250E+5	< 0.0001
Pure error	–	3.920E−3	9	4.356E−4	–	–
Cor. total	–	16578.72	29	–	–	–
		(R^2 = 0.912 and Adj R^2 = 0.805)				

the randomness of the result and the significant effect of the model terms to the response (Table 3). The "Lack of Fit *F* value" of 625,049.41 implies that the Lack of Fit is significant. There is only a 0.01% chance that a "Lack of Fit *F* value" this large could occur due to noise. Adequate precision measures the signal to noise ratio. A ratio larger than 4 is desirable. Adequate precision ratio of 12.349 shows an adequate signal. This model can be used to navigate the design space. The quadratic model was used to explain the mathematical relationship between the independent variables and the dependent response. The mathematical expression for the relationship between RB19 decolorization with the independent variables: pH, time, concentration, and H_2O_2/MgO NPs molar ratio is shown in terms of coded factors in Eq. (3):

$$Y = 79.51 - 13.34A + 6.40B - 41.28C + 1.20D - 11.53AD - 13.07BC + 1.81BD - 3.90CD + 5.35A^2 - 16.09B^2 - 91.49C^2 + 8.07D^2. \quad (3)$$

"Prob > *F*" less than 0.0500 indicates that the model terms are significant. Values greater than 0.1000 indicate that the model terms are not significant. Statistical analysis showed that the coefficients; *C*, *BC*, B^2, and C^2 were statistically significant. *F* value shown in Table 3 indicates that time (*F* value: 9.27) has the greatest effect on the AOP for RB19 decolorization followed by concentration and pH. Also, the interaction between concentration and time showed a high *F* value of 7.54 than the other interactions. The high value of the coefficient of determination (R^2 = 0.912) being a measure of the goodness of fit to the model indicates a high degree of correlation between the predicted response and the experimental responses. The adjusted R^2 (0.805) also confirmed the high correlation between the observed values and the theoretical values. From Fig. 4, it was also confirmed that the experimental (actual) values were very close to the predicted values. The coefficient of a factor reflects the effect of that particular factor while the coefficients of

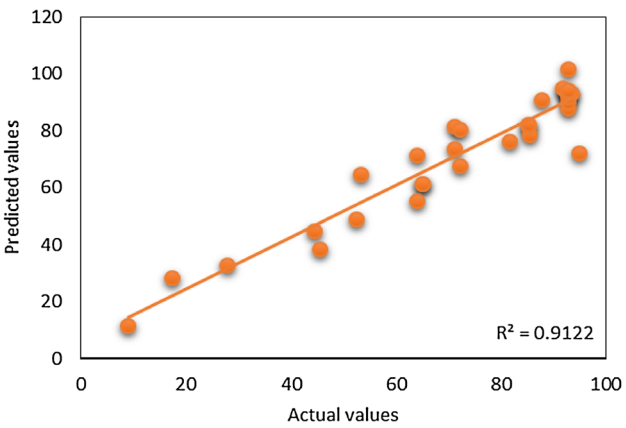

Fig. 4 Plot of the predicted values versus the observed values of RB19 decolorization

two combined factors show the interaction between them, whereas the second-order term indicates quadratic effect. The ANOVA results showed that the quadratic model (Eq. 3) is adequate to predict RB19 dye decolorization at the variables' studied range. A residual is defined as the change between an observed value, Y and it is fitted, $\hat{Y}$ [37]. Normal probability plot is used to check the normality distribution of the residuals [38]. Great deviation from normality was not observed in the normal probability plots of the residuals (Fig. 5).

Response surface plots

The interactive effects of the process variables on the RB19 decolorization using advanced process dye were studied further by plotting three-dimensional (3D) surface curves and two-dimensional (2D) figures against any two independent variables while keeping the other variables at their central (0) level. The 3D surface and 2D contours plots of the response (percentage decolorization) from the interactions between the variables are shown in Figs. 6, 7, 8, 9, 10 and 11. The pH is a very important parameter that actively

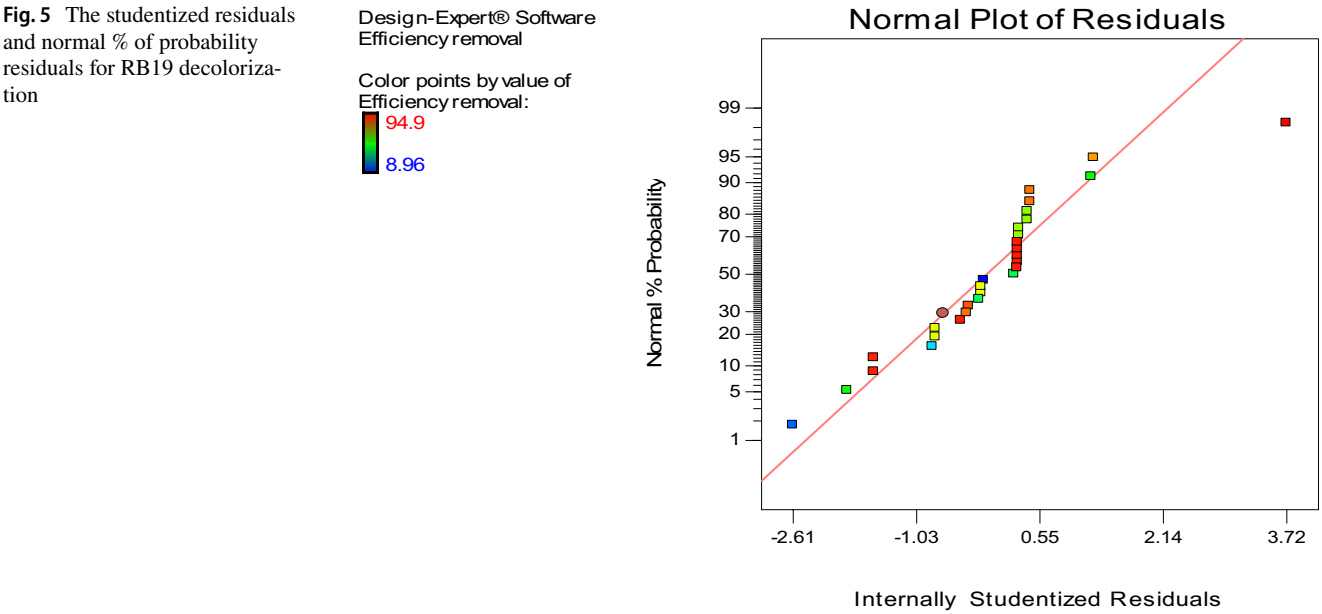

Fig. 5 The studentized residuals and normal % of probability residuals for RB19 decolorization

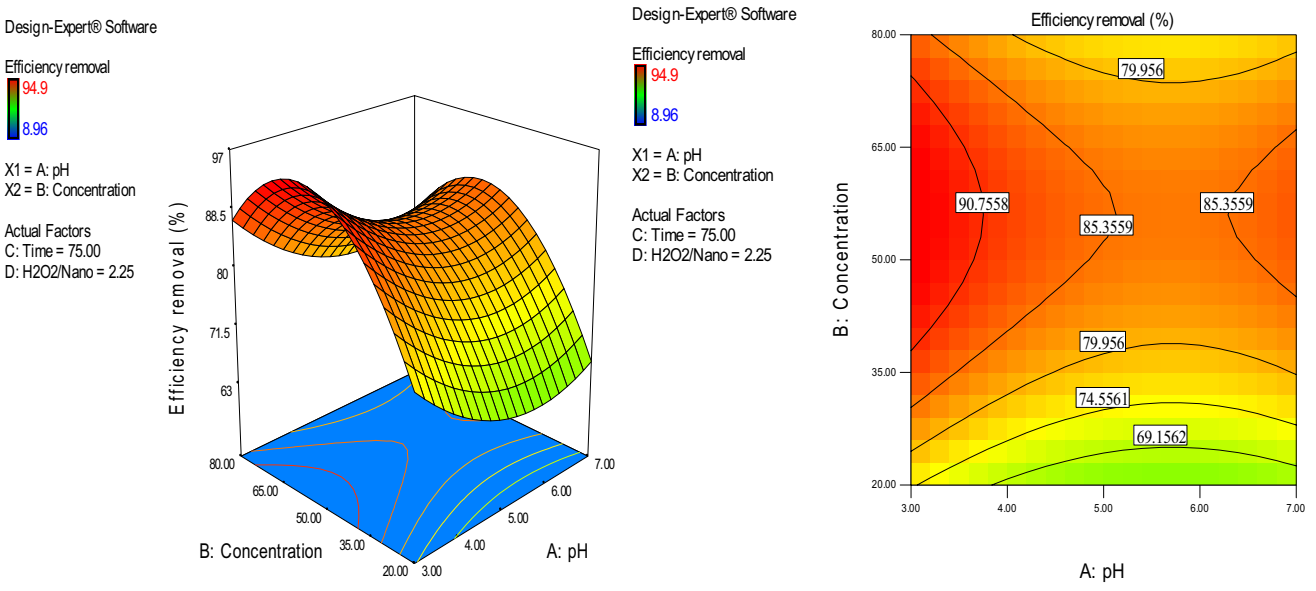

Fig. 6 3D surface and 2D contour plot of the interactive effect of pH and RB19 concentration on RB19 removal efficiency using advanced H_2O_2/MgO oxidation process at constant H_2O_2/MgO NPs ratio and time

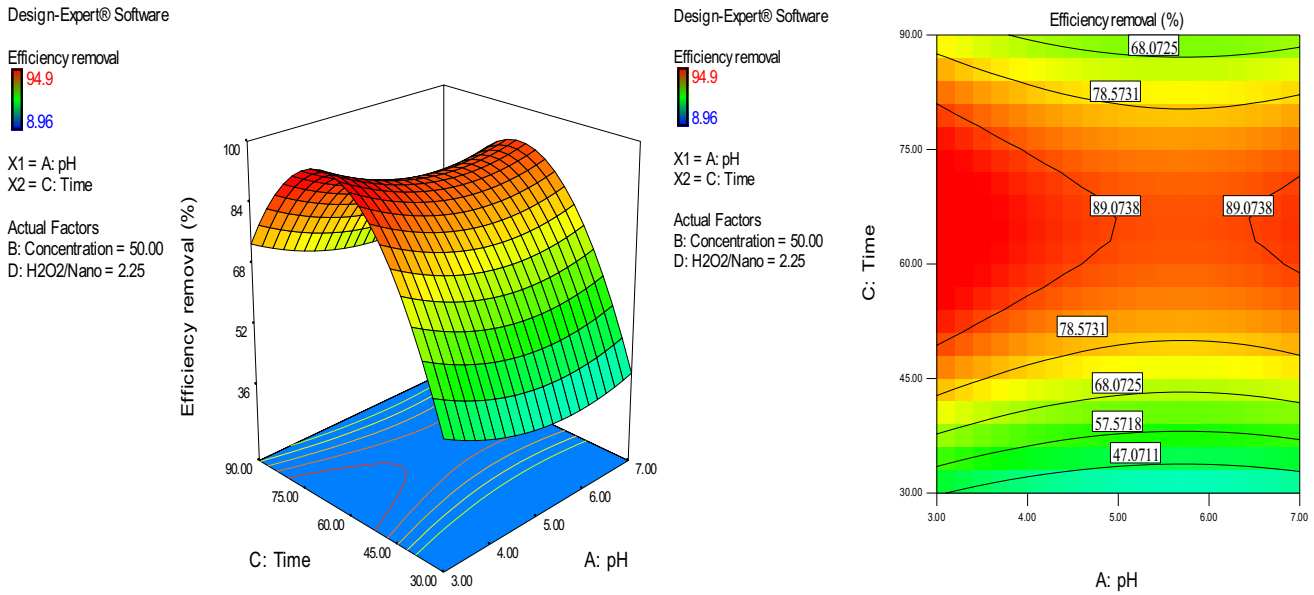

Fig. 7 3D surface and 2D contour plot of the interactive effect of pH and time on RB19 removal efficiency using advanced H_2O_2/MgO oxidation process at constant H_2O_2/MgO NPs ratio and RB19 concentration

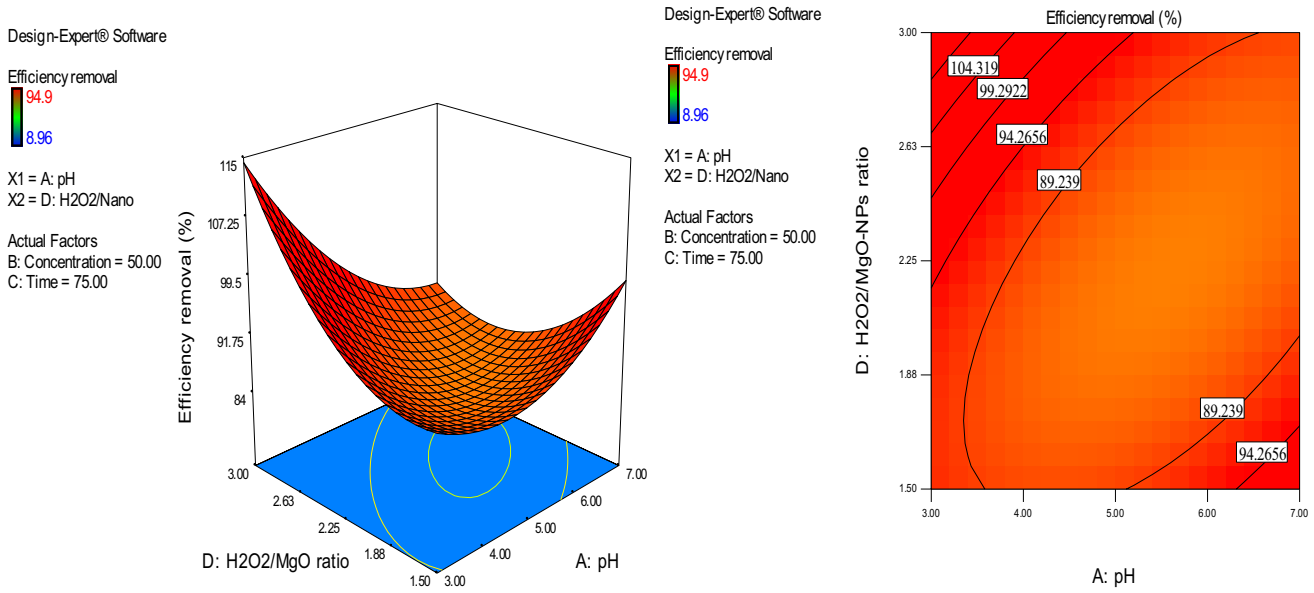

Fig. 8 3D surface and 2D contour plot of the interactive effect of pH and H_2O_2/MgO NPs ratio on RB19 removal efficiency using advanced H_2O_2/MgO oxidation process at constant RB19 concentration and time

affects the AOP. The effect of pH on RB19 decolorization is related to pH of the solution and the functional groups present in the MgO NPs, which affects its surface charge. Figure 6 shows that 90.5% decolorization was achieved at pH of 3.8 and concentration of 53.6 mg/L. 89% efficiency was observed at pH 4.3 and time of 67.8 min (Fig. 6). The percentage of decolorization was increased by decreasing the pH of the solution. However, it was observed that at higher pH, the decolorization of RB19 was reduced rapidly (Figs. 6, 7, 8). The solution pH is one of the parameters affecting the adsorbent level and ionization of pollutants [26, 34]. The impact of pH also depends on the zero point charge of the catalyst and acidity constant (pK_a). RB19 is an anionic dye and the value of pH_{ZPC} for MgO NPs was 12.4 [39]. Thus, MgO NPs at pH lowest of 12.4 had a positive charge. At pH higher than these values, MgO NPs had a negative charge.

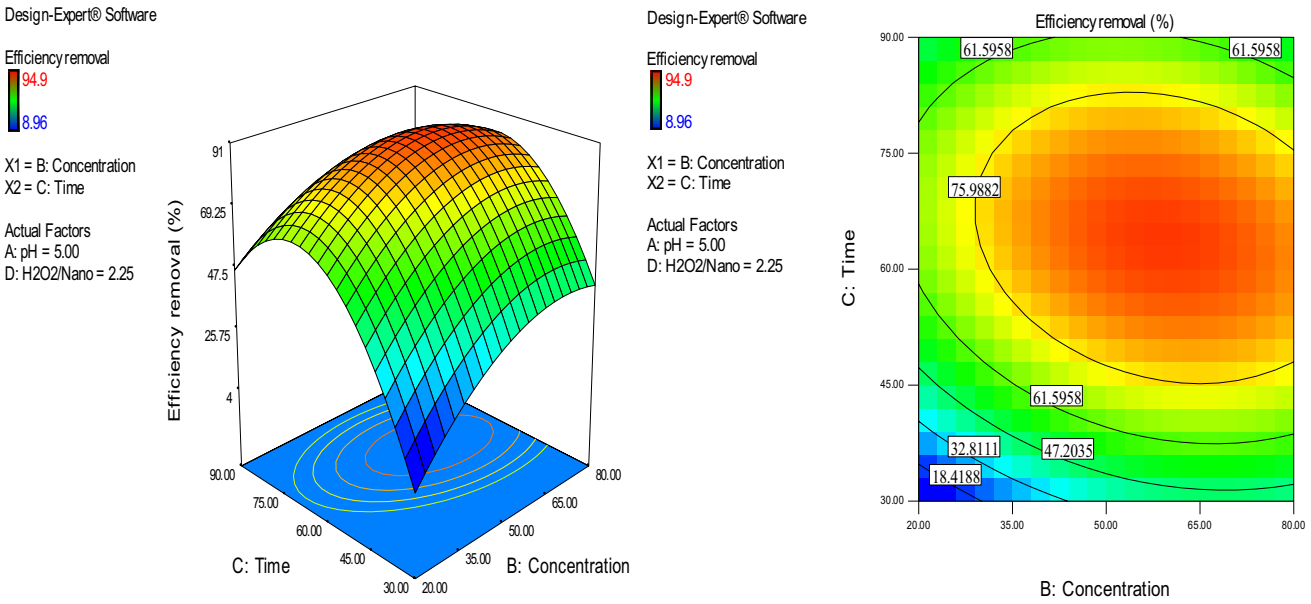

Fig. 9 3D surface and contour plot of the interactive effect of time and RB19 concentration on RB19 removal efficiency using advanced H_2O_2/MgO oxidation process at constant pH and H_2O_2/MgO NPs ratio

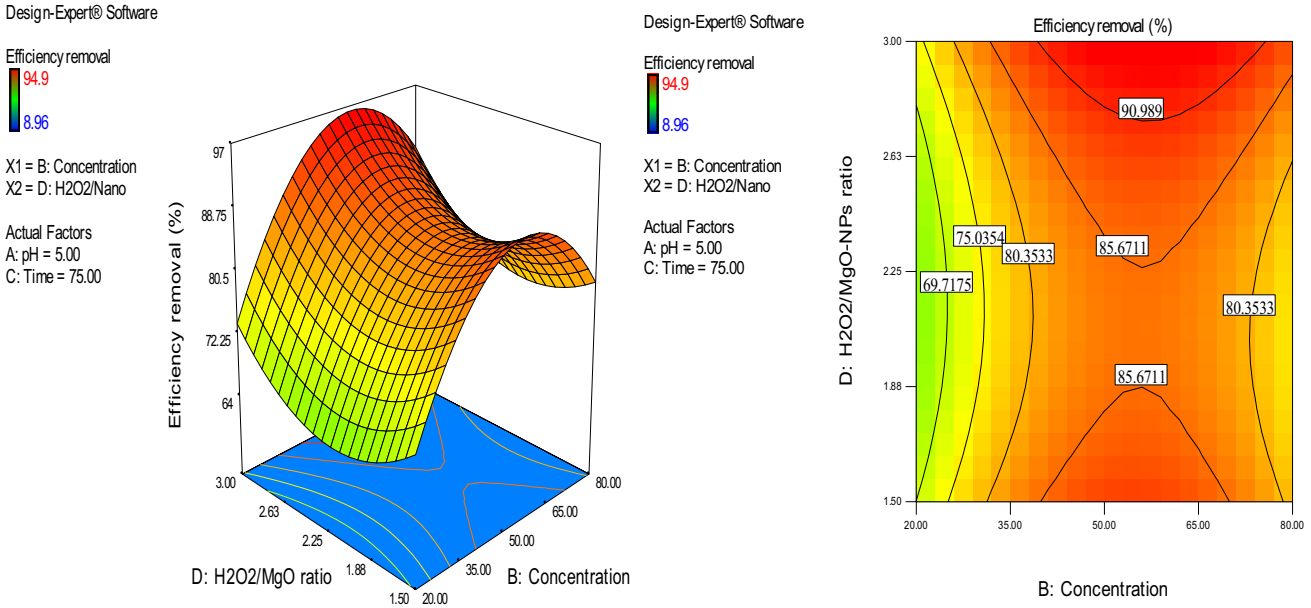

Fig. 10 3D surface and 2D contour plot of the interactive effect of H_2O_2/MgO NPs ratio and RB19 concentration on RB19 removal efficiency using advanced H_2O_2/MgO oxidation process at constant pH and time

But at pH above 12.4 and close to this value, the RB19 and nanoparticles had a neutral charge and leads to reduced efficiency. The cause of color decomposition in acidic pH is due to the instability of color rings with the presence of MgO NPs at the pH and the presence of H^+ on MgO NPs which resulted in better color reduction [30, 40]. Also, the decolorization of RB19 being favorable in the acidic environment is due to the electrostatic attractions between the negatively charged functional groups present on the anionic dye and the positively charged MgO NPs surface. A study that investigated the effect of nanoparticles on the treatment of dairy wastewater resulted in an optimum pH of 4 [41].

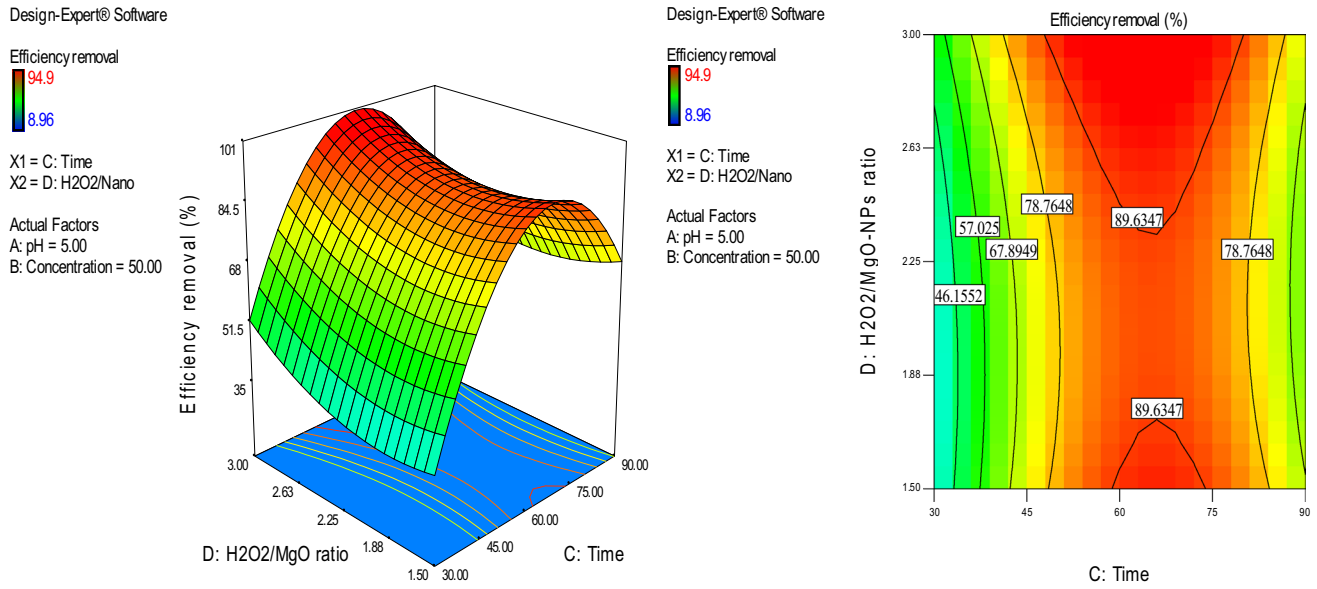

Fig. 11 3D surface and 2D contour plot of the interactive effect of H_2O_2/MgO NPs ratio and time on RB19 removal efficiency using advanced H_2O_2/MgO oxidation process at constant pH and RB19 concentration

The contact time is also important in all experimental processes. Figures 6, 9, and 11 show that higher amount of RB19 was decolorization at increased contact time. This is due to the high availability of the active sites with time. This is also due to an increase in the time leading to the production of radical hydroxyl needed for the reaction and these hydroxyl radicals will have enough time to react with organic compounds [42].

From Fig. 9, it can be seen that the RB19 concentration with time has a negative on the process. The removal efficiency was increased rapidly from contact time of 30–65 min. Previous studies have shown that the efficiency of removal is reduced at high concentrations due to saturation of the catalyst coating surface with the reacting compounds [43]. From the results obtained, in order to increase the efficiency at higher concentrations an increase in MgO NPs and $^{\cdot}OH$ in the reaction medium is required [44]. A higher rate of decolorization was observed at an H_2O_2/NPs ratio of 3. Studies have shown that the application of high molar ratios does not increase the efficiency of removal because higher molar ratios imply excess amounts of H_2O_2 react with $^{\cdot}OH$ radicals produced in the process and result in the production of weaker radicals that are less active than $^{\cdot}OH$. Hydroxyl radical in the reaction zone with H_2O_2 is combined in the environment and form scavenger radicals ($HO_2^{\cdot}$) that are weaker and contribute to the reduction of the removal efficiency [45, 46].

Optimization of RB19 decolorization

Optimization was done using the Design expert software (Stat-Ease, 7.1 trial version) to determine the optimum conditions for decolorization of RB19. Optimum conditions of pH 3, RB19 concentration of 80 mg/L, time of 60 min and H_2O_2/MgO NPs ratio of 3 were obtained, and the optimum decolorization efficiency at this optimum condition was predicted to be 93.77%. Experiment was carried out at these optimum conditions to validate the predicted optimum values. An experimental value of 92.93% was obtained, which was found to be in close agreement with the predicted percentage decolorization (93.77%). The desirability of a model close to unity and with low error depicts the applicability of the model [47]. A desirability of 0.973 (Fig. 12) confirms the applicability of the model and the predicted responses. Also, Fig. 13 shows the desirability effect of the individual process variables. Their desirability values are close to unity, which implies that each of the operating parameter satisfies the model. The values furthermore indicate how well each variable satisfies the model.

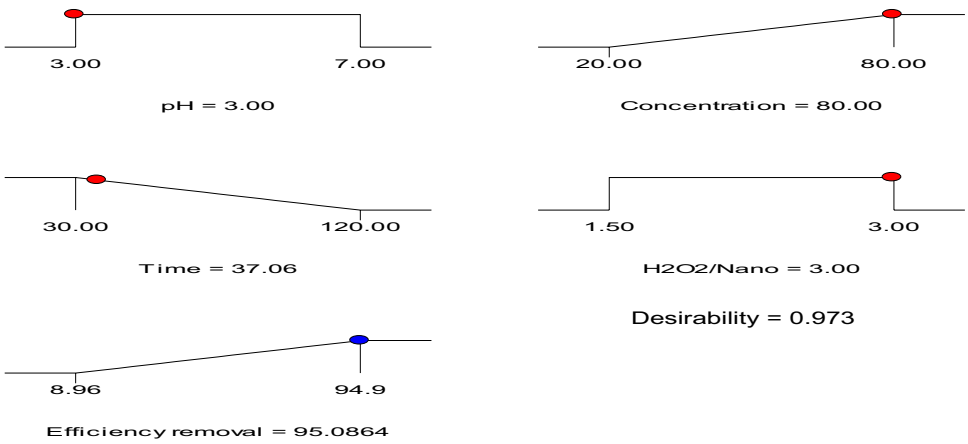

Fig. 12 The desirability effect for RB19 decolorization

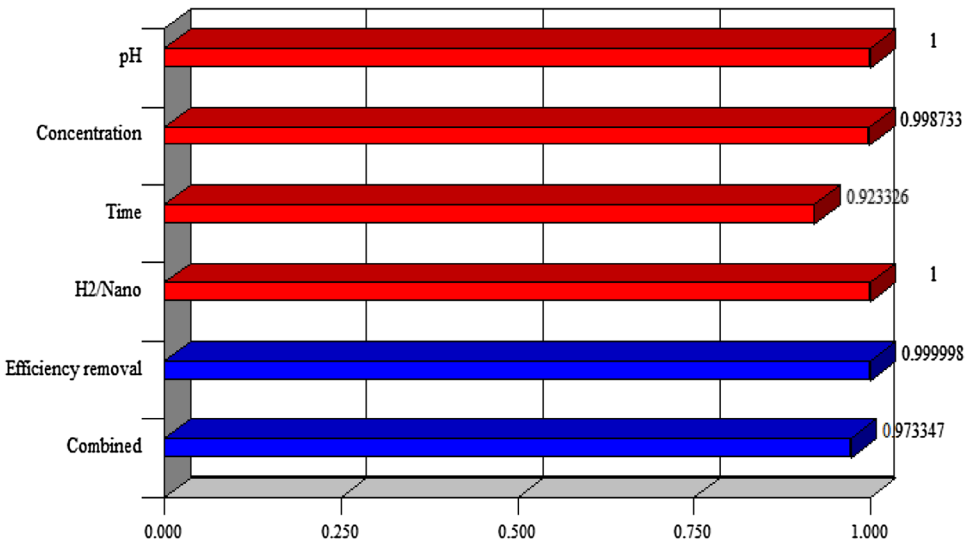

Fig. 13 Desirability effect of the individual operating parameter

Conclusions

The advanced H_2O_2/MgO oxidation process (AOP) removal of RB19 dye from aqueous solution was optimized using CCD in RSM. The effect of oxidation process parameters, pH (3–7), molar H_2O_2/MgO NPs ratio (1–3), initial concentration of RB19 (20–80 mg/L), and contact time (30–90 min) was investigated. The CCD of RSM was applied to study the interactive effects of the process parameters and the optimum conditions. A quadratic model equation relating the independent variables to the dependent variable was also generated from the design. One-way ANOVA was applied for statistical data analysis. The observed values were found to be very close to the predicted (theoretical) response values. Optimum conditions of pH 3, contact time of 60 min, RB19 concentration of 80 mg/L and H_2O_2/MgO NPs molar ratio of 3 were obtained, which gave RB19 removal efficiency of 93.77%. The value of the coefficient of determination ($R^2 = 0.912\%$) and adjusted R^2 (0.805%) showed that the removal of RB19 dye using AOP can be described by the RSM. The ANOVA results showed that the quadratic model developed from the RSM was statistically significant for RB19% decolorization. From the study, it was deduced that the RSM can be used for optimization of the process parameters for RB19 removal from aqueous solution and the advanced H_2O_2/MgO oxidation process.

Acknowledgements This work was supported by the Research Grant of the Environmental Health Laboratory of Zabol Province, Iran (Grant no. IR.ZBU. REC-1396-157).

Open Access This article is distributed under the terms of the Creative Commons Attribution 4.0 International License (http://creativecommons.org/licenses/by/4.0/), which permits unrestricted use, distribution, and reproduction in any medium, provided you give appropriate credit to the original author(s) and the source, provide a link to the Creative Commons license, and indicate if changes were made.

References

1. Paul SA, Chavan SK, Khambe SD (2012) Studies on characterization of textile industrial wastewater in Solapur city. Int J Chem Sci 10:635–642
2. Holkar CR, Jadhav AJ, Pinjari DV, Mahamuni NM, Pandit AB (2016) A critical review on textile wastewater treatments: possible approaches. J Environ Manag 182:351–366. https://doi.org/10.1016/j.jenvman.2016.07.090
3. Patel NB, Soni BD, Ruparelia JP (2000) Studies on removal of dyes from wastewater using electro-coagulation process. Nirma Univ J Eng Technol 1:24–30
4. Kobya M, Demirbas E, Can OT, Bayramoglu M (2006) Treatment of levafix orange textile dye solution by electrocoagulation. J Hazard Mater 132(2):183–188. https://doi.org/10.1016/j.jhazmat.2005.07.084
5. Golka K, Kopps S, Myslak ZW (2004) Carcinogenicity of azo colorants: influence of solubility and bioavailability. Toxicol Lett 151:203–210. https://doi.org/10.1016/j.toxlet.2003.11.016
6. Sanroman MA, Pazos M, Ricart MT, Cameselle C (2004) electrochemical decolourisation of structurally different dyes. Chemosphere 57:233–239. https://doi.org/10.1016/j.chemosphere.2004.06.019
7. Liu X, Qiu M, Huang C (2011) Degradation of the reactive black 5 by Fenton and Fenton-like system. Procedia Eng 15:4835–4840. https://doi.org/10.1016/j.proeng.2011.08.902
8. Ventura A, Jacquet G, Bermond A, Camel V (2002) Electrochemical generation of the Fenton's reagent: application to atrazine degradation. Water Res 36:3517–3522. https://doi.org/10.1016/S0043-1354(02)00064-7
9. Dalvand A, Gholami M, Ameri A, Mahmoodi NM (2011) Treatment of synthetic wastewater containing reactive red 198 by electrocoagulation process. Iran J Health Environ 4:11–22. https://doi.org/10.4103/2277-9183.196669
10. Muthukumar M, Karuppiah MT, Raju GB (2007) Electrochemical removal of CI Acid orange 10 from aqueous solutions. Sep Purif Technol 55:198–205. https://doi.org/10.1016/j.seppur.2006.11.014
11. Radaei E, Alavi Moghaddam MR, Arami M (2014) Removal of reactive blue 19 from aqueous solution by pomegranate residual-based activated carbon: optimization by response surface methodology. J Environ Health Sci Eng 12:65. https://doi.org/10.1186/2052-336X-12-65
12. Mahvi AH, Malakootian MR (2011) Comparison of polyaluminum silicate chloride and electrocoagulation process, in natural organic matter removal from surface water in Ghochan. Iran J Water Chem Technol 33:377–385
13. Bechtold T, Burtscher E, Turcanu A (2001) Cathodic decolorisation of textile wastewater containing reactive dyes using multicathode electrolyser. J Chem Technol Biotechnol 76:303–311. https://doi.org/10.1002/jctb.383
14. Chatterjee S, Lee DS, Lee MW, Woo SH (2009) Enhanced adsorption of congo red from aqueous solutions by chitosan hydrogel beads impregnated with cetyltrimethyl ammonium bromide. Bioresour Technol 100:2803–2809. https://doi.org/10.1016/j.biortech.2008.12.035
15. Ahmadi S, KordMostafapour F (2017) Treatment of textile wastewater using a combined coagulation and DAF processes, Iran, 2016. Arch Hyg Sci 6:229–234
16. Hosseini KE, Alavi Moghaddam MR, Hashemi SH (2012) Investigation of decolorization kinetics and biodegradation of azo dye Acid Red 18 using sequential process of anaerobic sequencing batch reactor/moving bed sequencing batch biofilm reactor. Int Biodeterior Biodegener 71:43–49. https://doi.org/10.1016/j.ibiod.2012.04.002
17. Daneshvar N, Aber S, Vatanpour V, Rasoulifard MH (2008) Electro-Fenton treatment of dye solution containing Orange II: influence of operational parameters. J Electroanal Chem 615:165–174. https://doi.org/10.1016/j.jelechem.2007.12.005
18. Rahdar S, Igwegbe CA, Rahdar A, Ahmadi S (2018) Efficiency of sono-nano-catalytic process of magnesium oxide nanoparticle in removal of penicillin G from aqueous solution. Desalin Water Treat 106:330–335. https://doi.org/10.5004/dwt.2018.22102
19. Liang SX, Jia Z, Zhang WC, Li XF, Wang WM, Lin HC, Zhang LC (2018) Ultrafast activation efficiency of three peroxides by $Fe_{78}Si_9B_{13}$ metallic glass under photo enhanced catalytic oxidation: a comparative study. Appl Catal B Environ 221:108–118. https://doi.org/10.1016/j.apcatb.2017.09.007
20. Ren C, Yang B, Wu M, Xu J, Fu Z, Guo T (2010) Synthesis of Ag/ZnO nanorods array with enhanced photocatalytic performance. J Hazard Mater 9:123–182. https://doi.org/10.1016/j.jhazmat.2010.05.141
21. Arsene D, Musteret CP, Catrinescu C, Apopei P, Barjoveanu G, Teodosiuc C (2011) Combined oxidation and ultrafiltration processes for the removal of priority organic pollutants from wastewaters. Environ Eng Manag J 10:67–76
22. Poulopoulos S, Arvanitakis F, Philippopoulos C (2006) Photochemical treatment of phenol aqueous solutions using ultraviolet radiation and hydrogen peroxide. J Hazard Mater 8:64–129. https://doi.org/10.1016/j.jhazmat.2005.06.044
23. Loures CC, Alcântara MA, IzárioFilho HJ, Silva FT, Paiva TC (2013) Advanced oxidative degradation processes: fundamentals and applications. Int Rev Chem Eng 5:102–120
24. Liang SX, Jia Z, Zhang WC, Li XF, Wang WM, Zhang LC (2017) Rapid malachite green degradation using $Fe_{73.5}Si_{13.5}B_9Cu_1Nb_3$ metallic glass for activation of persulfate under UV–Vis light. Mater Des 119:244–253. https://doi.org/10.1016/j.matdes.2017.01.039
25. Jia Z, Kang J, Zhang WC, Wang WM, Yang C, Sun H, Habibi D, Zhang LC (2017) Surface aging behaviour of Fe-based amorphous alloys as catalysts during heterogeneous photo Fenton-like process for water treatment. Appl Catal B 204:537–547. https://doi.org/10.1016/j.apcatb.2016.12.001
26. Wang JC, Jia Z, Liang SX, Qin P, Zhang WC, Wang WM, Sercombbe TB, Zhang LC (2018) $Fe_{73.5}Si_{13.5}B_9Cu_1Nb_3$ metallic glass: rapid activation of peroxymonosulfate towards ultrafast Eosin Y degradation. Mater Des 140:73–84. https://doi.org/10.1016/j.matdes.2017.11.049
27. Yazdanbakhsh AR, Manshouri M, Sheikhmohmmadi A, Sardar M (2012) Investigation the efficiency of combined coagulation and advanced oxidation by Fenton process in the removal of clarithromycin and antibiotics COD. J Water Wastewater 23:22–29
28. Mesdaghinia AR, Farrokhi M, Nasseri S, Yazdanbakhsh AR (2004) Biodegradation enhancement of 2,4,6 trichlorophenol (TCP) by Fenton oxidation process. J Hakim Sci 7:33–42
29. Nga NK, Hong PTT, Lam TD, Huy TQ (2013) A facile synthesis of nanostructured magnesium oxide particles for enhanced adsorption performance in Reactive Blue 19 removal. J Colloid Interface Sci 398:210–216. https://doi.org/10.1016/j.jcis.2013.02.018

30. Khoshnamvand N, Ahmadi S, Mostafapour FK (2017) Kinetic and isotherm studies on ciprofloxacin adsorption using magnesium oxide nanoparticles. J Appl Pharm Sci 7:079–083. https://doi.org/10.7324/JAPS.2017.71112
31. Yoosefian M, Ahmadzadeh S, Aghasi M, Dolatabadi M (2017) Optimization of electrocoagulation process for efficient removal of ciprofloxacin antibiotic using iron electrode: kinetic and isotherm studies of adsorption. J Mol Liq 225:544–553. https://doi.org/10.1016/j.molliq.2016.11.093
32. Ahmadi S, Banach A, Mostafapour FK, Balarak D (2017) Study survey of cupric oxide nanoparticles in removal efficiency of ciprofloxacin antibiotic from aqueous solution: adsorption isotherm study. Desalin Water Treat 89:297–303. https://doi.org/10.5004/dwt.2017.21362
33. Ahmadi S, Mostafapour FK (2017) Survey of efficiency of dissolved air flotation in removal Penicillin G from aqueous solutions. Brit J Pharm Res 15:1–11. https://doi.org/10.9734/BJPR/2017/31180
34. Mohamadi L, BazrafshanE Noroozifar M, Ansari-Moghaddam A (2016) Ethylbenzene removal from aqueous environments by catalytic ozonation process using MgO nanoparticles. J Mazandaran Univ Med Sci 26:129–144
35. Onyechi CA (2014) Textile wastewater treatment using activated carbon from agro-wastes. Master of Engineering Thesis. Department of Chemical Engineering, Nnamdi Azikiwe University, Awka, Nigeria
36. Agarry SE, Owabor CN (2012) Evaluation of the adsorption potential of rubber (*Hevea brasiliensis*) seed pericarp-activated carbon in abattoir wastewater treatment and in the removal of iron(II) ions from aqueous solution. Niger J Technol (NIJOTECH) 31:346–358
37. Montgomery DC (2005) Design and analysis of experiments, 6th edn. Wiley, New York
38. Ghanim AN (2014) Optimization of pollutants removal from textile wastewater by electrocoagulation through RSM. J Babylon Univ Eng Sci 22:375–378
39. Tak BY, Tak BS, Kim YJ, Park YJ, Yoon YH, Min GH (2015) Optimization of color and COD removal from livestock wastewater by electrocoagulation process: Application of Box–Behnken design (BBD). J Ind Eng Chem 28:307–315. https://doi.org/10.1016/j.jiec.2015.03.008
40. Jia Z, Wang JC, Liang SX, Zhang WC, Wang WM, Zhang LC (2017) Activation of peroxymonosulfate by $Fe_{78}Si_9B_{13}$ metallic glass: the influence of crystallization. J Alloys Compd 728:525–533. https://doi.org/10.1016/j.jallcom.2017.09.019
41. De Abreu P, Pereira EL, Campos CMM (2012) Photocatalytic oxidation process ($UV/H_2O_2/ZnO$) in the treatment and sterilization of dairy wastewater. Acta Sci Technol 35:75–81. https://doi.org/10.4025/actascitechnol.v35i1.11132
42. Javid A, Nasseri S, Mesdaghinia A, Mahvi A, Alimohammadi M, Aghdam RM (2013) Performance of photocatalytic oxidation of tetracycline in aqueous solution by TiO_2 nanofibers. J Environ Health Sci Eng 11:2–6. https://doi.org/10.1186/2052-336X-11-24
43. NikKheslat A, Amin M (2011) Study on photocatalytic degradation of phenol by a process of oxidation in the presence of titanium dioxide batch ultraviolet radiation. In: Fourteenth national conference of environmental health medicine University of Yazd, Yazd, Iran
44. Noori Motlagh Z, Shams Khoramabadi GH, Godini H (2013) The efficiency of photocatalytic process of ZnO nanoparticles on methylene blue bleaching and COD removal from synthetic wastewater. Lorestan Sci J 14:51–61
45. Parastar S, Pooreshgh Y, Nasseri S (2013) Investigation of photocatalytic removal of nitrate from aqueous solution using the ZnO/UV. Heal Environ J 3:54–61
46. Roslan J, Mustapa Kamal SM, Md. Yunos KF, Abdullah N (2015) Optimization of enzymatic hydrolysis of tilapia (*Oreochromis niloticus*) by-product using response surface methodology. Int Food Res J 22:1117–1123
47. Shahzad N, Pugliese D, Cauda V, Shahzad MI, Shah Z, Baig MA, Tresso E (2017) Comparative spectroscopic approach for the dye loading optimization of sheet-like ZnO photoanodes for dye-sensitized solar cells. J Photochem Photobiol A Chem 337:192–197. https://doi.org/10.1016/j.jphotochem.2017.01.011

Publisher's Note Springer Nature remains neutral with regard to jurisdictional claims in published maps and institutional affiliations.